Behavior of a Two-Span Continuous Plate Girder Bridge Designed by the Alternate Load Factor Method

MARK MOORE and MICHAEL A. GRUBB

SUMMARY

A large experimental test program to evaluate the behavior of a continuous plate-girder bridge with precast prestressed deck panels, designed according to Alternate Load Factor (Autostress) procedures, has been conducted at the FHWA Turner-Fairbank Highway Research Center in McLean, Virginia. The project was sponsored jointly by the American Iron and Steel Institute (AISI) and the Federal Highway Administration (FHWA). A 0.4 scale model of a two-span continuous plate-girder bridge was subjected to a series of tests at each of the three AASHTO load levels—Service Load, Overload, and Maximum Load. At the Service Load level, elastic lateral live-load distribution was studied. At the Overload and Maximum Load levels, the adequacy of the Alternate Load Factor Design limit-state criteria to satisfy related structural performance requirements was analyzed. Deck panel behavior was studied at all three load levels.

The prototype bridge had two equal spans of 140 ft, an overall width of 48 ft with three girders spaced at 17 ft, and 10-in. thick composite modular precast deck panels prestressed in the transverse and longitudinal directions. The girders were designed using Alternate Load Factor (Autostress) procedures. Alternate Load Factor Design (ALFD) is a limit-states design approach that more realistically approximates the actual behavior of continuous steel members at higher loads than present design procedures. ALFD recognizes and takes advantage of the ability of continuous steel members to adjust automatically for effects of controlled local yielding. An AASHTO guide specification presently permits the use of ALFD for braced compact sections. This model bridge study is part of a comprehensive research program to extend ALFD procedures to non-compact girders with slender webs.

The model bridge consisted of three plate girders, with two 56-ft spans, transversely spaced at approximately 6 ft 9 in. and supporting 4-in. prestressed modular deck panels with approximately 2 ft 10 in. overhangs. Each plate girder was approximately 28-in. deep and was made composite with the deck panels using stud shear connectors.

Preliminary test results from the model bridge study are presented. Experimentally determined elastic girder wheel-load distribution factors at the Service Load level are compared to factors computed from finite-element results, recently developed empirical formulas, and present AASHTO procedures. Limit-state criteria introduced to continuous-bridge design in ALFD, such as the formation of automoments and the shakedown phenomenon at Overload, are illustrated experimentally, along with the ability of these criteria to satisfy the structural performance requirements at Overload. The available reserve strength at Maximum Load is analyzed, as well as the adequacy of the mechanism analysis allowed in the ALFD procedures for strength prediction.

Mark Moore is senior engineer with Wiss, Janney, Elstner Associates, Inc.

Michael A. Grubb is assistant manager—bridge engineering with AISC Marketing, Inc.

INTRODUCTION

In late 1982, a large jointly funded bridge-research program was initiated between the AISI and the FHWA. The primary purpose of this program was to study experimentally the behavior of a scale model of a two-span continuous plate-girder bridge designed according to ALFD procedures.[1] An equally important objective of the project was to study the behavior of a bridge with composite modular precast deck panels prestressed in both the transverse and longitudinal directions.

In ALFD, a designer is permitted to utilize some of the substantial post-yielding reserve strength that is available in composite continuous steel-girder bridges. The concepts of shakedown at Overload and plastic mechanism analysis at Maximum Load are introduced in ALFD as more realistic limit-state criteria for continuous steel bridges under heavy loads.[2] Currently, an AASHTO guide specification[3] permits the use of ALFD for the design of continuous bridges using rolled-beam and comparable welded-beam sections that satisfy specific compactness requirements. The first bridges designed according to this guide specification were built in New York and Tennessee. The cost of both bridges was substantially less than for bridges designed by conventional procedures.[4,5] Additional projects are now underway in Maine and Illinois.

The model-bridge study is part of an extensive research program in progress to extend the ALFD concepts to non-compact plate-girder sections with slender webs that fall outside the compactness limits of the present guide specification.[6–9] The experimental study involved the laboratory testing of a 0.4 scale model of a two-span continuous steel-girder highway bridge. The prototype bridge was designed by indus-

Table 1.
Performance Requirements and Limit-State Criteria

Loading	Structural Performance Requirements	Limit State Criteria
Dead Load	• Adjust for long-term deformations	• For unshored construction, precamber for dead load, plus automoments,* plus differential creep and shrinkage
Service Load	• Adequate fatigue life • Control elastic deflections • Limit concrete cracking	• Stress range < specified limits • Live load deflection < L/800 • Zero tension in concrete slab*
Overload	• Control permanent deformations to ensure a smooth ride	• Shakedown with automoments • Limit tensile stress in slab to $5\sqrt{f_c'}$* • Limit stress in positive bending < $0.95F_y$ after forming automoments
Maximum Load	• Permit at least one passage of the load	• Mechanism shall not form • Avoid uplift

* These limit state criteria apply to this bridge only.

try personnel using ALFD procedures, and will be discussed in more detail in the next section. The model bridge consisted of two 56-ft spans each with three plate girders transversely spaced at approximately 6 ft 9 in. Each plate girder was approximately 28-in. deep. The girders supported 4 in. thick modular precast concrete deck panels with approximately 2 ft 10 in. overhangs. The precast panels were made composite with the plate girders using stud shear connectors. The panels were prestressed both transverse and parallel to the bridge axis. Components for the bridge were fabricated in two commercial shops, and erected by a steel fabricator in the structures laboratory at the FHWA Turner-Fairbank Highway Research Center in McLean, Virginia. Details of the design, fabrication, erection, and test plan for the model bridge have previously been reported.[10,11] Construction of the model bridge was completed in April 1987.

A comprehensive test plan, Fig. 1, was developed with the objective of evaluating specific responses of the model bridge at each of the three distinct AASHTO load levels—Service Load, Overload, and Maximum Load. These load levels are used in ALFD and in the present AASHTO limit-states design approach known as Load Factor Design (LFD).[12] Specific structural performance requirements must be satisfied at each of these load levels. The structural performance requirements for each load level are summarized in Table 1.

The model-bridge test plan included specific tasks to

TASK A: Erect steel girders and cross frames. Install and check steel-girder instrumentation.
TASK B: Apply compensatory noncomposite dead load (DL1) to the steel girders.
TASK C: Erect precast slabs and post-tension longitudinally. Grout the panels to the steel girders.
TASK D: Apply composite dead load (DL2) to the model bridge.
TASK E: Determine elastic influence surfaces for pier sections and maximum positive moment sections.
TASK F: Determine elastic lateral load distribution to the exterior and interior girders in positive and negative bending at Service Load.
TASK G: Transfer the dead loads and dead-load load fixtures to the top of the model bridge deck panels.
TASK H: Apply single concentrated loads to study lateral load-distribution behavior for exterior and interior girders in positive and negative bending before shakedown at Overload.
TASK I: Apply simulated Overload truck loads (plus impact) in positive-bending regions before automoment formation.
TASK J: Apply simulated Overload lane loads (plus impact) to form automoments.
TASK K: Re-apply simulated Overload truck loads (plus impact) in positive-bending regions to observe shakedown after automoment formation.
TASK L: Re-apply single concentrated loads to compare lateral load-distribution behavior for exterior and interior girders in positive and negative bending before and after shakedown at Overload.
TASK M: Remove selected cross frames and repeat selected tasks to study the effect of the cross frames on lateral load distribution.
TASK N: Install additional transverse stiffeners on each girder at half the web depth from each side of the interior pier and repeat selected Overload tests.
TASK O: Compensate for lost dead load and apply additional dead load (DL3) to approximate the theoretical increase in dead load at Maximum Load.
TASK P: Apply simulated Maximum Load lane loads (plus impact).
TASK Q: Apply simulated lane loads past Maximum Load (plus impact) until the bridge can resist no more load.
TASK R: Perform punching shear tests on the precast deck panels.

Fig. 1. Detailed test plan for model bridge study.

develop elastic influence surfaces and live-load lateral distribution factors at Service-Load stress levels. The goal was to compare girder live-load distribution factors computed from the experimental data with factors computed using present AASHTO procedures, mathematical finite-element models, and recently developed empirical formulas.[13] The adequacy of the live-load distribution theory conventionally used for concrete deck-slab design was to be studied as well. Specific tasks were also to be completed at simulated Overload and Maximum Load levels to observe the ability of the ALFD limit-state criteria to satisfy the related structural performance requirements at each load level for non-compact plate-girder sections. These tasks will be discussed in more detail in later sections. In addition, localized deck-panel tests and tests to bridge failure were completed. The two-year test program was completed in April 1989. Testing in the laboratory was accomplished by FHWA personnel. Data analysis is the responsibility of AISI. This paper provides an overview of the research program and provides some results from preliminary data analysis at each load level.

DESCRIPTION OF THE PROTOTYPE BRIDGE

For the purposes of the model-bridge study, a prototype bridge was designed using ALFD procedures. The specific limit-state criteria imposed at each load level in the prototype design are summarized in Table 1. The prototype bridge configuration used was a two-span continuous structure with equal spans of 140 ft. Overall deck width was 48 ft. The roadway width of 44 ft 6 in. allowed for three design lanes. The deck consisted of uniform 10-in. thick precast concrete panels 8 ft wide by 48 ft long. Mechanical leveling and hold-down devices were used to position and secure the panels during erection and post-tensioning. The transverse joints between panels were a double-female configuration filled with grout after panel installation, but before longitudinal post-tensioning. The panels were prestressed (pre-tensioned) transverse to the bridge roadway with two layers of straight strands in the 48-ft direction. Galvanized corrugated metal ducts were provided at mid-depth in each panel across the 8-ft dimension for post-tensioning the panels along the full length of the bridge, parallel to the longitudinal centerline. The ducts were grouted following the post-tensioning operation. Block-outs were provided in the panels for installation of stud shear connectors. After the panels were longitudinally post-tensioned and the shear connectors installed, the block-outs and girder-to-panel interfaces were grouted to make the panels composite with the girders along the full length. The specified ultimate 28-day concrete compressive strength for the panels was 6000 psi. Prestressing of the panels was accomplished using $\frac{7}{16}$-in. diameter strand in the transverse direction and using 0.60-in. diameter strand in the longitudinal direction. All strand was 270 ksi stress-relieved low relaxation strand. A total prestress of 1,200 psi was required for the longitudinal post-tensioning to satisfy the deck-panel limit-states at Service Load and Overload, including effects of differential creep and shrinkage.

The superstructure consisted of three parallel flange (68-in. web depth) steel plate girders spaced at 17 ft, with a deck overhang beyond the exterior girders of 7 ft. This arrangement provided good lateral elastic load balance between the three girders. Unpainted ASTM A588 weathering steel, 50 ksi nominal yield strength, was assumed. These features—wider girder spacing resulting in a minimum number of girders in the cross section, and unpainted A588 steel—are two of the most significant contributors to the cost-effectiveness of plate-girder bridges.[14] The bridge was designed for AASHTO HS20 live loading plus the alternate military loading specified by AASHTO for bridges on the Interstate System. An AASHTO Case I roadway was assumed for checking fatigue. The prototype bridge was also designed using improved live-load lateral distribution factors generated from a three-dimensional finite-element analysis of the bridge using the MSC/NASTRAN[15] program. Live-load distribution factors developed for one-lane loaded were used to check fatigue details for over 2,000,000 cycles of truck loading, as specified by AASHTO for a Case I roadway. The improved live-load distribution factors showed some significant reduction over factors computed using present AASHTO procedures, particularly for the interior girder, and will be discussed in more detail later.

Because the prototype bridge girders were designed using ALFD procedures, it was possible to use a prismatic girder section over the interior pier for this particular bridge configuration. ALFD procedures recognize the ability of continuous steel members to adjust automatically for effects of controlled local yielding at Overload. A portion of the peak elastic bending moment at interior piers is automatically redistributed by the structure to lower-stressed positive-moment sections due to local yielding. Taking advantage of this inherent ability permits the designer to consider using prismatic steel members in continuous spans along the entire bridge length or between the field splices. The concomitant benefits include lower fabrication costs and elimination of structural details with undesirable fatigue characteristics. Because a modified plastic mechanism analysis[16] is also introduced in ALFD procedures at Maximum Load, Overload or serviceability criteria typically govern the design under the present AASHTO load factors. This appears more rational since it is probable that a bridge will be subjected to Overload-type vehicles during its life. Also, continuous steel bridges have a great deal of reserve strength at Maximum Load due to load redistribution, both longitudinally along the girder and transversely between girders, that is not adequately taken advantage of by present LFD Maximum Load limit-state criteria.

The bottom (compression) flanges of the prototype bridge girders over the interior pier were designed as ultracompact flanges. An ultracompact flange is defined[9] as being com-

pact for plastic design according to criteria given in Part 2 (Plastic Design) of the American Institute of Steel Construction (AISC) specification for buildings.[17] For a specified nominal yield strength of 50 ksi, an ultracompact compression flange has a maximum allowable projecting flange slenderness ratio of 7.0. Recent research has indicated that non-compact girder sections in negative bending utilizing ultracompact compression flanges can deliver much improved inelastic-rotation capacities at Maximum Load.[9]

The time-varying effects of differential creep and shrinkage of the prestressed modular deck panels against the steel girders were also considered in the design of the prototype bridge. The chosen method of approach is well known[18] and accounts for the time-varying effects of creep and shrinkage as they affect the steel girders. The result was a slight increase in the amount of panel prestressing required to satisfy the limit states and some additional camber in the steel girders. The effects of differential creep and shrinkage are seldom considered in general bridge design practice but were considered in this study because of the research nature of the project.

DESCRIPTION OF THE MODEL BRIDGE

The dimensions of the model bridge were determined by the physical characteristics of the FHWA Structures Laboratory, fabrication techniques, and availability of plate material. Based on these limitations, a 0.4-scale factor was selected. Design of the model bridge was largely a process of applying the scale factor to the prototype bridge components, rounding to practical dimensions, and detailing. The model bridge had two 56-ft spans, a transverse girder spacing of 6 ft 9⅝ in., and 2-ft 9$^{9}/_{16}$-in. deck-panel overhangs. A typical cross section is shown in Fig. 2 and an elevation view of one span in Fig. 3.

Girders

The top flange of each girder was ¼ in. by 5⅝ in. throughout. The web of each girder was ¼ in. by 27$^{3}/_{16}$ in. throughout. The bottom flange of each girder was $^{9}/_{16}$ in. by 8 in. throughout, except 11 ft 2 in. from the abutments where the flange thickness decreased to $^{5}/_{16}$ in. All the above dimensions are nominal dimensions.

Bearing stiffeners were located on both sides of the web over the supports of each girder. Cross-frame connection plates were located at 10-ft intervals, measured from the abutments, along the interior girder on both sides of the web, and along each exterior girder on the inside face of the web only. These full-depth stiffeners were rigidly connected to the girder top and bottom flanges as required by AASHTO, using fillet welds. The cross frames were comprised of vee-shaped diagonals, top and bottom horizontal members, and a vertical post, all WT2×6.5 rolled sections. The cross frame members were welded to the gusset plates which were bolted to the connection plates. Because only a limited number of rolled tee sections were available, the cross-frame members were not scaled-down exactly from the prototype bridge. An attempt was made to determine the effect of this in specific tasks of the test plan. In addition, two intermediate transverse stiffeners were located within the 10-ft web panels adjacent to the abutments and in 10-ft panels adjacent to the field splices. The 6-ft panels directly on either side of the interior pier each contained two intermediate transverse stiffeners. The stiffener in each panel closest to the interior pier was located a distance of half the web depth from the pier section and was fillet welded to the bottom (compression) flange. These closely spaced stiffeners, added to each girder in the latter stages of the test program, have also been shown to contribute greatly to improved inelastic-rotation capacities for non-compact sections in negative bending at Maximum Load.[9] In addition, these additional stiffeners limit web distortions at Overload. All the intermediate transverse stiffeners were one sided and were terminated 1 in. short of the tension flange. All stiffeners, except the closely spaced stiffeners, were cut from plates and welded with a continuous fillet weld to the web. The closely spaced stiffeners were rolled 2½ in.×2½ in.×$^{5}/_{16}$ in. angles and were bolted to the web with ASTM A325 high-strength bolts according to the criteria given in Reference 19. The bolted angles were used here only to simulate welded plate stiffeners and for their relative ease of installation. The thickness of the intermediate transverse-stiffener plates and cross-frame connection plates was $^{5}/_{16}$ in., and the thickness of the bearing-stiffener plates was ¼ in. at the abutments and $^{11}/_{16}$ in. at the interior pier. All gusset plates for the cross frames were ¼-in. thick.

Each girder had a bolted field splice 14 ft 3 in. on each

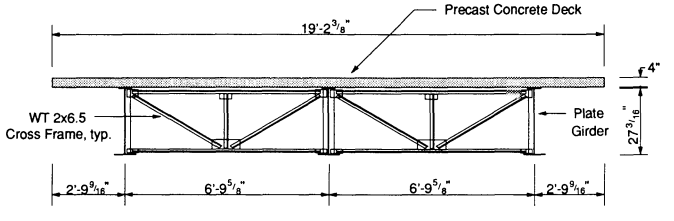

Fig. 2. Cross section of model bridge.

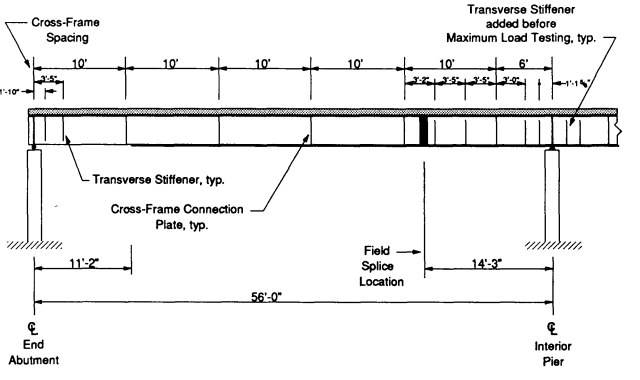

Fig. 3. Elevation of model bridge.

side of the interior pier composed of ¼-in. splice plates fastened with ¾-in. diameter ASTM A325 high-strength bolts. Each girder was supported on roller bearings at both abutments and on a fixed bearing permitting rotation but no translation at the interior pier. Each end-abutment bearing was a 2-in. diameter roller placed between two ¾-in. sole plates. The interior-pier bearing consisted of a ¾-in. sole plate, a plate with a rounded top surface, and two pintels. The top sole plates were welded to the bottom flanges of the girders while the bottom sole plates rested on circular load cells supported on concrete piers. The load cells were used to measure the girder reactions at each bearing. Instrumentation on the steel girders included numerous strain gages, deflection transducers, and rotation gages.

Material tests were conducted on specimens taken from the actual plate material to determine the static yield strengths of the webs, flanges, and stiffeners. Because it was desired to achieve average measured static yield strengths as close as possible to the specified nominal yield strength of 50 ksi and actual measured yield strengths are often higher than the specified nominal yield strength, ASTM A36 material was used for the girders. The average measured static yield strengths of the plate material used in the model bridge varied from 42.1 ksi to 55.9 ksi.

Precast Panels

The 35 modular precast deck panels on the model bridge each were 4-in. thick, 3 ft 2 in. wide, and 19 ft 2 in. long. The deck panels were pretensioned in the transverse direction using $\frac{7}{16}$-in. diameter strand and post-tensioned along the full length of the bridge after erection using 0.6-in. diameter strand. The panel-to-panel joints were grouted prior to post-tensioning. After post-tensioning, a 28-day waiting period was observed to allow for some of the concrete creep and shrinkage to occur before making the panels composite with the girders. Grout was then placed in the $\frac{5}{16}$-in. separation between the top of the girders and the bottom of the deck panels, and in each pocket around the ⅝-in. diameter 3-in. long stud shear connectors, to achieve composite action. Leveling and hold-down devices were provided as specified in the prototype design. Two additional test panels were cast to obtain independent data on concrete creep and shrinkage. Instrumentation in the panels included strain gages mounted on mild reinforcement bars embedded in the panels and numerous surface mounted Whittemore points.

The average compressive strength of the concrete in the panels varied from 6520 psi to 8020 psi over the duration of testing. The average measured ultimate strength of the $\frac{7}{16}$-in. diameter prestressing strand was 281.7 ksi, and the average yield strength measured at 1 percent elongation was 247.8 ksi. The average measured ultimate strength of the 0.60-in. diameter prestressing strand was 271.8 ksi, and the average yield strength measured at 1 percent elongation was 253.6 ksi. Measured yield strengths for both the $\frac{7}{16}$-in. and 0.60-in. diameter strands exceeded the minimum requirement for yield strength of 90 percent of the rated strand capacity for low-relaxation strand specified in ASTM A416.

COMPENSATORY DEAD LOADS

Dead-load stresses in a scale model are smaller than dead-load stresses in a prototype if both are constructed with the same material. For the model-bridge study, actual dead-load stresses in the model bridge were only 40 percent of the dead-load stresses in the prototype bridge. To satisfy the rules of similitude, it was important to model the critical dead-load moments and shears as closely as possible. However, the exact simulation of the additional dead load that needed to be added to the model bridge, as a true uniform load, was not practical. Instead, concentrated loads were applied to each girder at three locations in each span to simulate a compensatory uniform dead load. The loads were applied at approximately the four-tenths, six-tenths, and eight-tenths point in each span of each girder, measured from the abutments. Compensatory noncomposite dead loads (DL1) were applied to the bottom flanges of the steel girders at these locations immediately after erection of the steel framing. These loads were maintained as constant as possible during deck-panel erection. In addition to the DL1 loads, compensatory composite dead loads (DL2), which include the effects of the barrier curbs, railings, and future wearing surface, were also applied to the bottom flanges of the steel girders after the deck panels were erected, post-tentioned, and made composite with the girders. This total load was maintained during the Service Load testing. The total compensatory load was then transferred from the girder bottom flanges to the top of the precast panels at the completion of the Service-Load testing and maintained for the remainder of the test program.

The magnitudes of the concentrated compensatory dead loads were determined to give approximately the same critical elastic dead-load moments and shears as in each girder of the prototype (scaled down). The elastic DL2 moments and shears in the prototype were computed assuming that the DL2 load was distributed equally to each girder, as allowed by AASHTO. All compensatory loads were computed using elastic influence coefficients determined from a three-dimensional MSC/NASTRAN finite-element model of the model bridge. The compensatory DL1 loads are shown in Fig. 4. The weight of the model bridge after erection was 127.5 kips (including the weight of the deck panels). An additional 150.4 kips was added to the model bridge to approximately scale the critical DL1 moments and shears correctly. The total DL1 load of 277.9 kips was slightly less than the total DL1 load on the prototype (scaled down) because less concentrated load is needed to produce a given moment than uniform load to produce the same moment. The compensatory DL2 loads, which total 60.8 kips, are shown in Fig. 5.

Additional dead load (termed DL3) also had to be added

to the composite model bridge between the Overload and Maximum Load testing. This additional load of 98.0 kips simulated the theoretical 30 percent increase in dead load specified by AASHTO at Maximum Load. The concentrated DL3 loads that were applied are shown in Fig. 6. In all cases, it was not necessary to apply compensatory loads at each location, as illustrated in Figs. 4 through 6. Using all these compensatory loads, elastic dead-load pier moments, maximum span moments, and pier shears in each girder of the model bridge compared favorably with the corresponding MSC/NASTRAN elastic dead-load moments and shears in the model bridge.

The measured dead-load reactions at each bearing of the model bridge after steel erection are shown in Fig. 7. Total measured dead-load reactions, minus the measured reactions due to self-weight of the steel in Fig. 7, are compared with the total dead-load reactions from the MSC/NASTRAN finite-element model after the addition of the compensatory DL1 loads, Fig. 8, after erection, post-tensioning and grouting of the precast panels, Fig. 9, and after the addition of the compensatory DL2 loads, Fig. 10. As shown in Fig. 9, about 29 percent of the compensatory DL1 load was unintentionally relieved during erection of the precast panels, presumably during welding of the stud shear connectors to the girders. This loss was later compensated for between the Overload and Maximum Load testing. During Overload testing, the reduced dead-load level was compensated for by increasing the simulated live loads and will be discussed later.

SERVICE LOAD TESTING

Lateral live-load distribution behavior of the model bridge at elastic Service-Load stress levels was evaluated in a series of tests. Following erection and instrumentation of the model bridge, elastic influence surfaces were generated. Subsequently, elastic lateral live-load distribution to the interior and exterior girders in both positive and negative bending was determined by loading the bridge with scaled-down AASHTO HS vehicle axle lines. At the completion of Overload testing, selected cross frames were removed and portions of the Service-Load testing were repeated. Data from these two latter tasks have not yet been analyzed. Only the initial influence surface tests are reported below. In addition, only live-load distribution to the girders is considered here and deck-panel distribution behavior is not discussed. The experimental program did not include fatigue testing at Service Load.

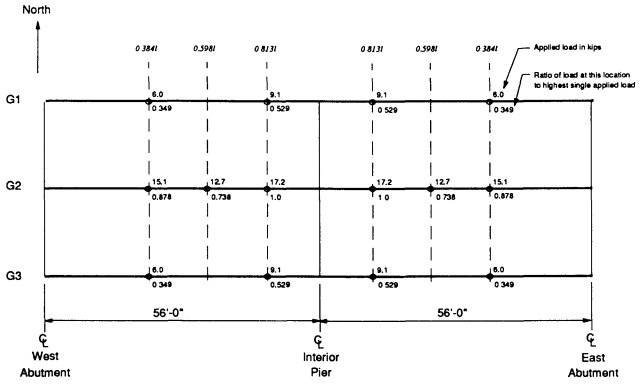

Fig. 4. Compensatory Dead Load 1 (DL1) applied to the non-composite model bridge after steel erection.

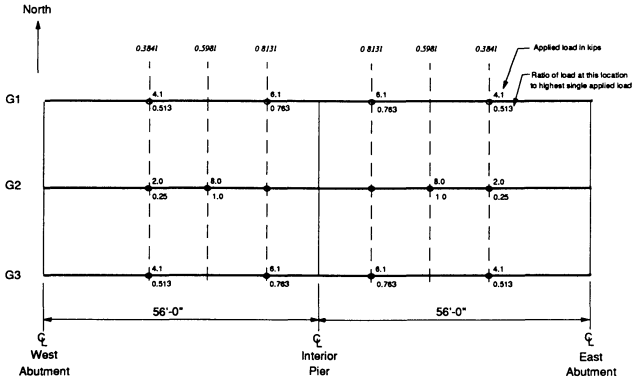

Fig. 5. Compensatory Dead Load 2 (DL2) applied to the composite model bridge after deck panels made composite with steel girders.

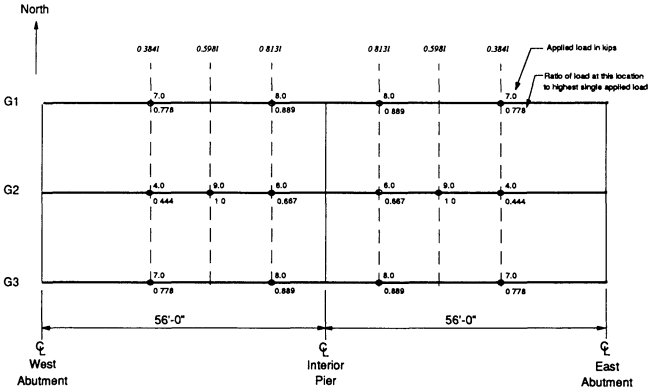

Fig. 6. Compensatory Dead Load 3 (DL3) applied to the composite model bridge before Maximum Load testing.

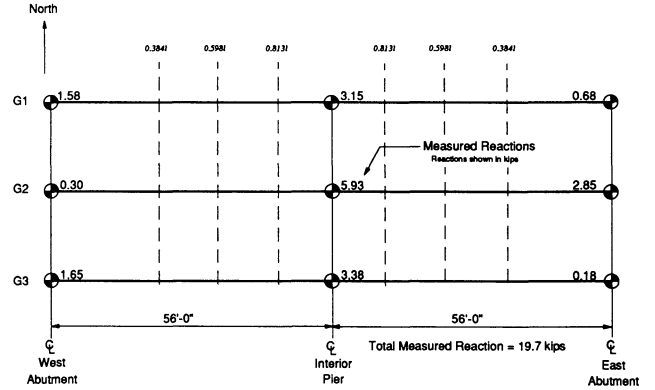

Fig. 7. Measured reactions after erection of steel girders and cross frames.

Elastic Influence Surface Test

In the elastic influence surface test, the elastic forces in the bottom flange of each girder at the interior-pier sections, and the maximum positive moment sections due to a single concentrated load, were measured experimentally, and compared with the corresponding theoretical elastic bottom-flange forces computed from the MSC/NASTRAN finite-element model of the model bridge. The bottom-flange forces were used as a measure of the bending moment in each girder. The measured forces were then used to compute elastic lateral live-load girder distribution factors according to a method reported previously.[20] These factors were compared to: (1) factors computed from the corresponding MSC/NASTRAN forces using the same method; (2) factors computed from proposed empirical formulas developed in an ongoing related National Cooperative Highway Research Program (NCHRP) study;[13] and (3) factors computed using present AASHTO procedures.

A single concentrated load of 16.6 kips, made up of lead weights, Fig. 11, was applied at locations spaced approximately one-fifth of the span along the full length of the bridge to generate the influence surfaces. The magnitude of the weight was selected so that measurable strains could be recorded while not causing yielding in the girders. In the transverse direction, the applied load was placed at locations near the edge of the deck overhangs, directly over each girder, and halfway in-between each girder. Fig. 12 illustrates the locations of the applied load for the elastic influence surface test. Lateral live-load distribution factors for the model bridge were then developed from the experimental data. Lateral distribution factors vary somewhat along the span. This variation is ignored in present and proposed specifications. To illustrate, distribution factors for both interior and exterior girders at critical positive-moment and negative-moment regions of the bridge were computed.

To determine the critical distribution factor in the positive-moment region, measured bottom-flange forces at the four-tenths point of the west span of the exterior and interior

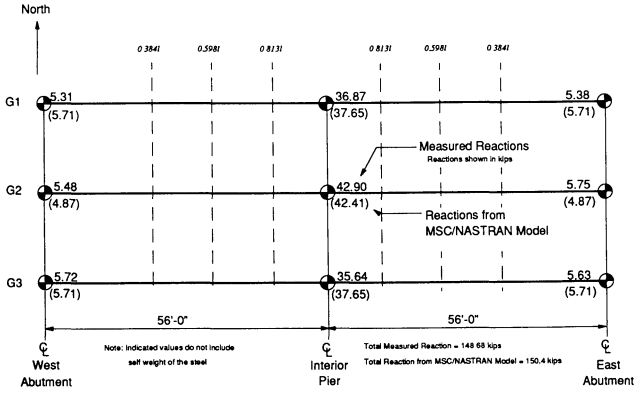

Fig. 8. Comparison of measured reactions after application of compensatory Dead Load 1 (DL1) and predicted values from MSC/NASTRAN finite element model.

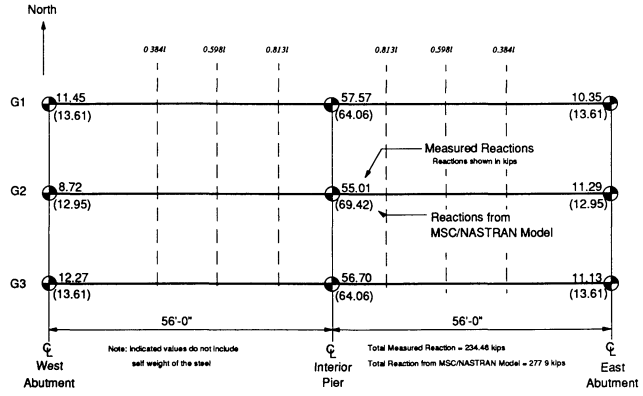

Fig. 9. Comparison of measured reactions after erection, post-tensioning, and grouting of precast deck panels and predicted values from MSC/NASTRAN finite element model.

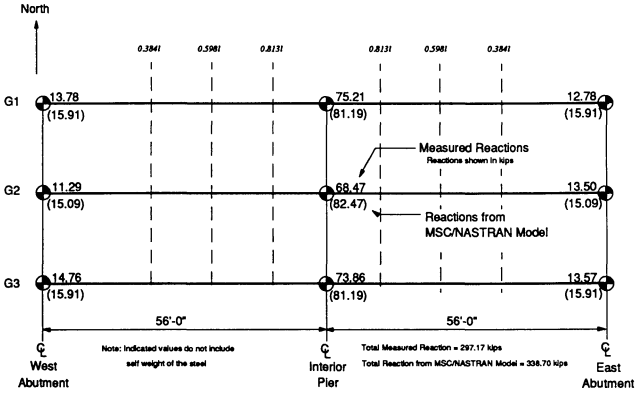

Fig. 10. Comparison of measured reactions after application of compensatory Dead Load 2 (DL2) to the composite model bridge and predicted values from MSC/NASTRAN finite element model.

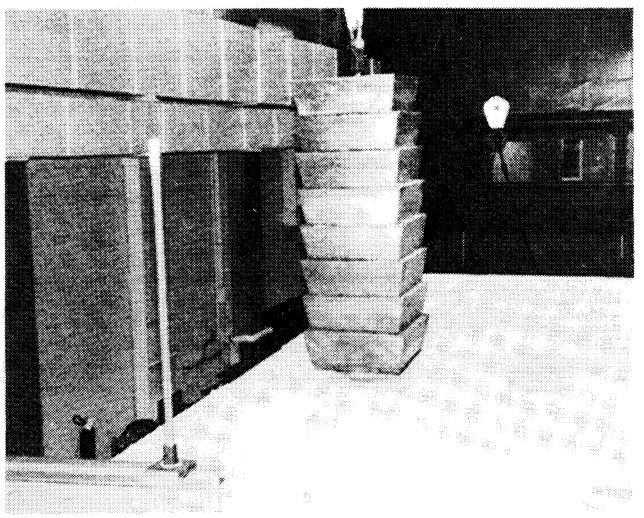

Fig. 11. 16.6 kip lead weight used for elastic influence surface testing.

girders (measured from the abutment) due to the 16.6 kip concentrated load applied across the section at the four-tenths point in the west span were computed and plotted in Figs. 13 and 14, respectively. Also shown in each figure are the corresponding bottom-flange forces from the finite-element model. For both the exterior and interior girders, excellent correlation between the experimental test data and the analytical solution was observed.

Similarly, to determine the critical distribution factor in the negative-moment region, measured bottom-flange forces at the interior pier in the exterior and interior girders due to the 16.6 kip load applied across the section at the six-tenth point of the west span (measured from the abutment) were computed and plotted in Figs. 15 and 16, respectively. Loading at the six-tenth points was assumed to be critical for the interior pier. These forces were also compared to the corresponding bottom-flange forces from the analytical model. Reasonable correlation between the measured data and the finite-element solution was observed. For both the interior and exterior girders, however, the finite-element analysis generally overestimated the lateral stiffness of the bridge and predicted flange forces less than those actually measured. This effect was more pronounced at the interior pier.

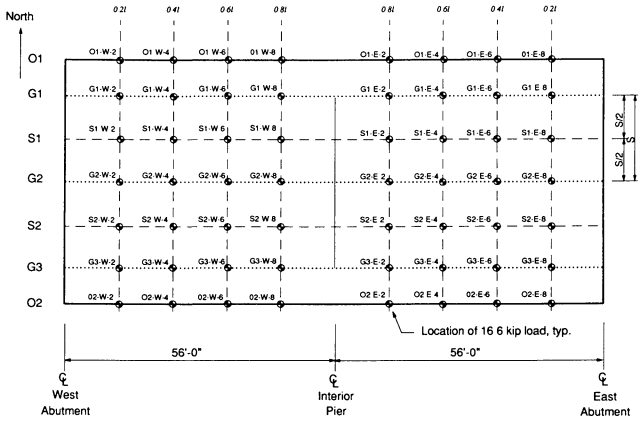

Fig. 12. Plan view of model bridge showing the locations of the applied load during the elastic influence surface test.

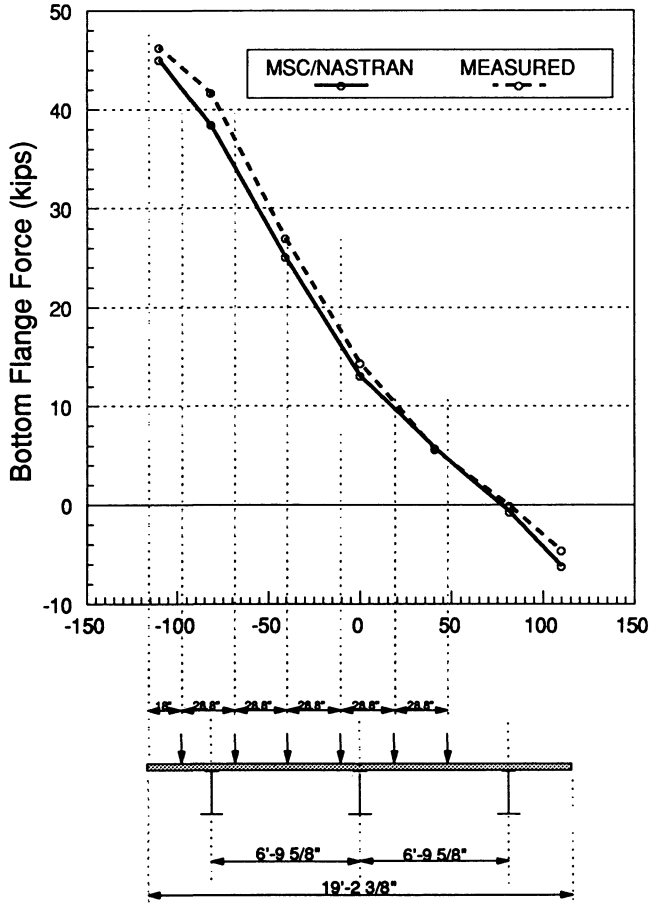

Fig. 13. Comparison of bottom-flange forces at 0.4l (west span) from measured test data and the finite-element model for an exterior girder with the 16.6 kip load applied across the section at 0.4l (west span).

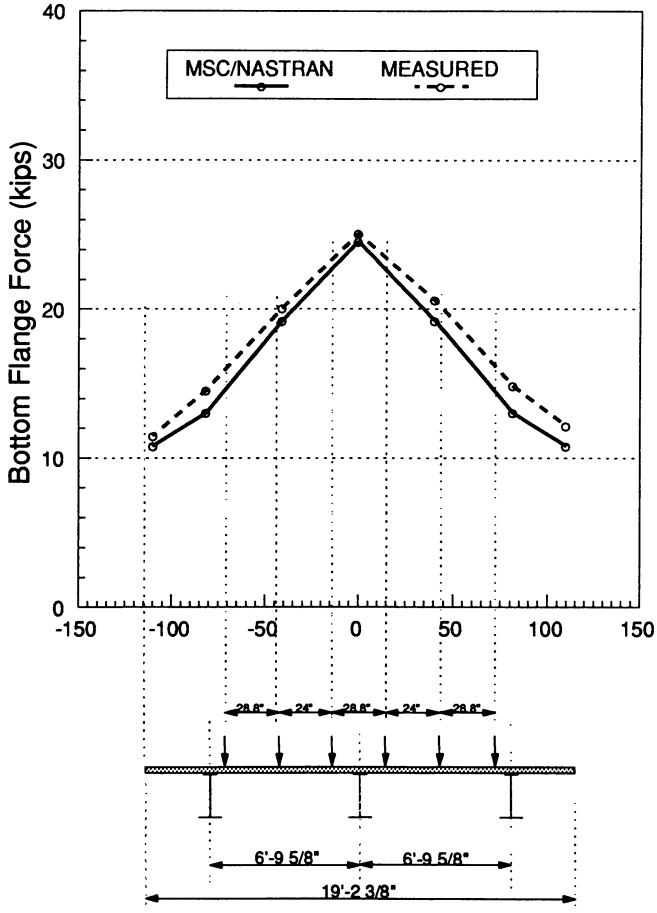

Fig. 14. Comparison of bottom-flange forces at 0.4l (west span) from measured test data and the finite-element model for an interior girder with the 16.6 kip load applied across the section at 0.4l (west span).

Once the plots discussed above were developed, the total bottom-flange force at each location due to a single axle line of AASHTO HS vehicles could be computed. At the bottom of each figure, a scaled-down single axle line for three lanes of AASHTO HS vehicles is shown. For each girder, the axles are shifted in their design lanes according to AASHTO rules to cause the worst loading on that girder. From each plot, contributing bottom-flange forces under each wheel are summed for one, two, and three lanes loaded. For three lanes loaded, the sum is reduced by 10 percent as allowed by AASHTO to account for the probability of coincident loading. Each sum is then divided by the theoretical elastic bottom-flange force at either the four-tenths point of the span or the interior pier from a single line-girder finite-element model to determine the corresponding distribution factor.[20]

Table 2 summarizes the wheel load distribution factors computed from the experimental data using the above method. In addition, Table 2 lists for comparison the wheel-load distribution factors computed with data from the MSC/NASTRAN finite-element model using the same method, factors computed according to the current AASHTO specification procedures, and factors computed from empirical formulas proposed in NCHRP Project 12-26. The agreement between the factors computed from the experimental and MSC/NASTRAN data is well within 10 percent in most cases. The larger deviation in the experimental and MSC/NASTRAN factors for the exterior girder at the interior pier will be investigated further as more data is later analyzed. The AASHTO factors appear to be quite conservative for the interior girder and less so for the exterior girder. The factors from the proposed empirical formulas give good agreement for the interior girder but do not differentiate between two and three lanes loaded. A separate formula does exist to compute factors for one lane loaded, however, The proposed method presently uses the same procedure to compute distribution factors for exterior girders as AASHTO (assuming the deck to act as a simple span between the girders). As shown, the observed variation in the distribution factor along the span is not considered in either the present or proposed methods.

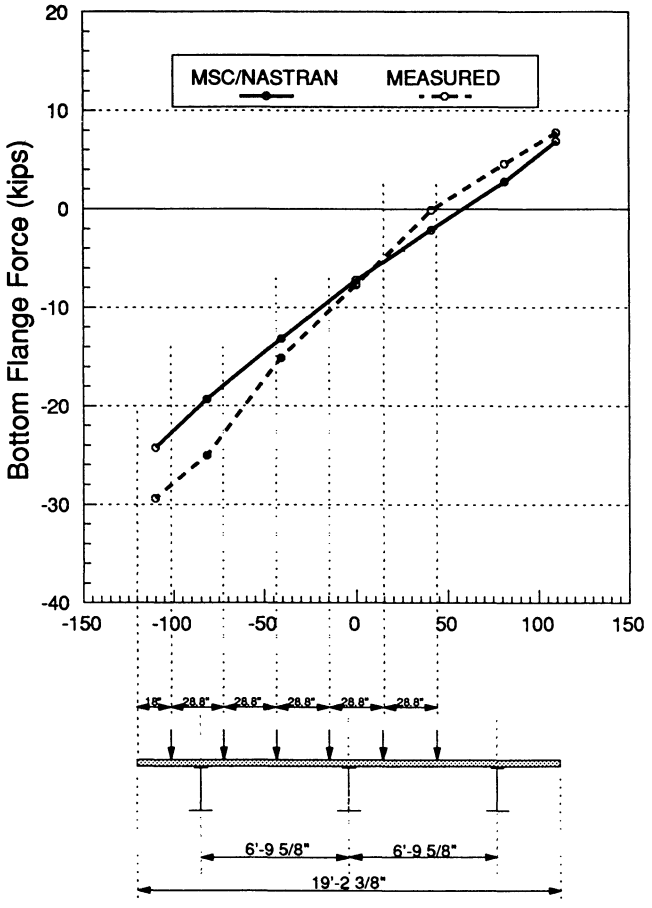

Fig. 15. Comparison of bottom-flange forces at the interior pier from measured test data and the finite-element model for an exterior girder with the 16.6 kip load applied across the section at 0.6l (west span).

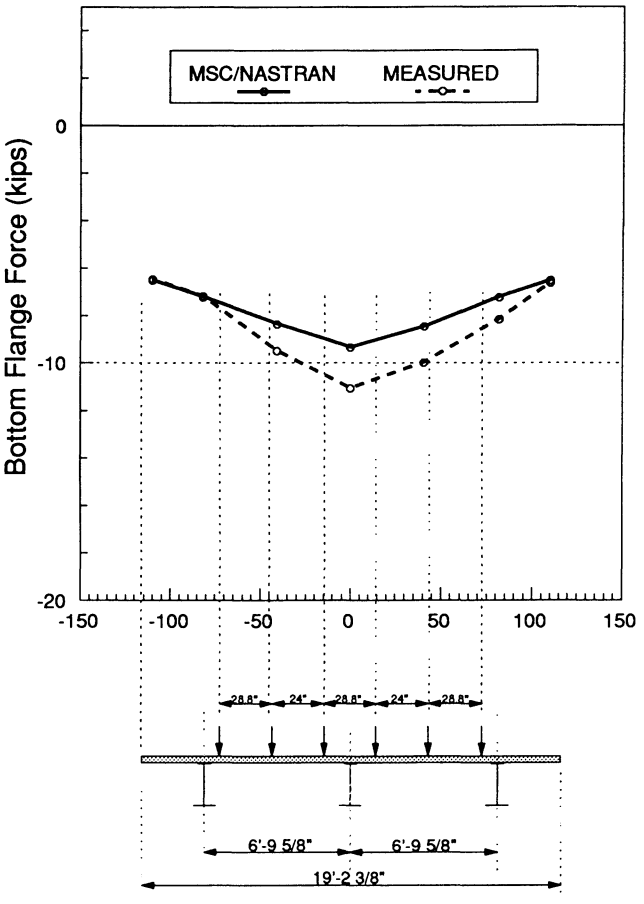

Fig. 16. Comparison of bottom-flange forces at the interior pier from measured test data and the finite-element model for an interior girder with the 16.6 kip load applied across the section at 0.6l (west span).

Table 2.
Comparison of Girder, Wheel-Load Lateral Distribution Factors Computed from Test Data, Finite-Element Analysis, Current Specifications, and Proposed Empirical Formulas

			Experimental Data	MSC/NASTRAN Finite Element Model	Current AASHTO Specifications	NCHRP 12-26 Proposal by Imbsen
At 0.41 of Span	Exterior Girder	One Lane	1.580	1.474	2.029	2.029
		Two Lanes	2.438	2.246	2.647	2.647
		Three Lanes	2.457	2.253	—	—
	Interior Girder	One Lane	0.909	0.930	1.647	1.027
		Two Lanes	1.613	1.600	2.824	2.122
		Three Lanes	2.076	2.043	2.806	2.122
At Interior Pier	Exterior Girder	One Lane	2.125	1.662	2.029	2.029
		Two Lanes	3.217	2.526	2.674	2.647
		Three Lanes	3.083	2.484	—	—
	Interior Girder	One Lane	0.883	0.867	1.647	1.027
		Two Lanes	1.646	1.532	2.824	2.122
		Three Lanes	2.115	1.977	2.806	2.122

OVERLOAD TESTING

At Overload, the single structural performance requirement is unobjectionable riding quality. To accomplish this, permanent deformations must be controlled. In ALFD, this requirement is satisfied by permitting a continuous-span bridge to shakedown.[1] Controlled local yielding is permitted at interior-pier sections at Overload which results in the formation of a set of self-equilibrating reactions and positive automoments that remain in the bridge after the live load is removed, Fig. 17. The local yielding is generally limited to the bottom (compression) flange and lower part of the web; a plastic hinge does not form.

The automoments act to reduce the peak negative elastic support moments and increase the smaller positive elastic span moments. Thus, the automoments cause a favorable redistribution of the elastic Overload moments. After several cycles of loading, the final automoment distribution is established. Because of these automoments, the bridge eventually behaves elastically again (shakes down) after several cycles of Overload; the controlled local yielding in the girders is stabilized. A bridge may never by subjected to heavy enough loads to form the design automoments, and such behavior is acceptable.

To control permanent deformations in the spans, the maximum stresses in positive bending are limited to $0.95F_y$ (for composite sections) after formation of the automoments. This limit state is retained from the AASHTO LFD method. Because the bridge eventually shakes down (behaves elastically), the stress limit state of $0.80F_y$ imposed in negative bending at Overload in LFD is not imposed in ALFD. Since Overload typically governs ALFD designs under the present AASHTO load factors, numerous flange thickness changes are therefore generally not required over interior

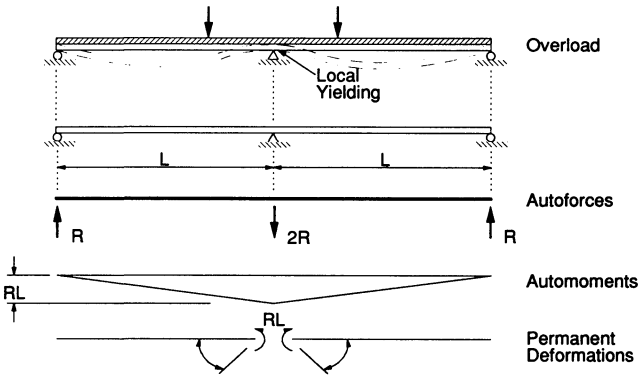

Fig. 17. Automoment diagram and permanent deformations.

piers to satisfy artificial-peak elastic Overload support moments that cannot be established due to local yielding. This contributes to reduced fabrication costs and improved fatigue behavior.

The small permanent deformations in each span due to the automoments (generally comparable to the composite dead-load deflections) are calculable and may be included in the dead-load camber to satisfy the structural performance requirement, as was done in the model bridge. To limit concrete cracking, ALFD procedures require that the mild reinforcement over interior-pier sections be properly distributed. In addition, ALFD requires that the reinforcement over the interior piers remain elastic at Overload. The requirement that the reinforcement remain elastic is intended to ensure that any deck cracks close after the live load is removed. This requirement can generally be satisfied by specifying Grade 60 reinforcement. In design of the model bridge, cracking of the precast panels over the interior pier was controlled instead by establishing levels of transverse and longitudinal panel prestressing to ensure that the concrete stresses in the panels did not exceed $5\sqrt{f_c'}$ at Overload. This requirement was in addition to a requirement imposed for this project that there be no tensile stress in the panels at Service Load.

To illustrate the principle of shakedown and observe the formation of automoments in the model bridge, the bridge was subjected to several cycles of simulated rated AASHTO Overload vehicles. At this rated Overload, the bridge should theoretically shake down (behave elastically) after several cycles of loading with the maximum positive-bending section in the most heavily loaded girder at a stress level equal to the limit state of $0.95F_y$ (including the stress due to the automoments). The behavior of the girders and precast deck-panels was observed after shakedown at this limit state to determine if the bridge adequately satisfied the structural performance requirement.

Development of Applied Loads

Different live-load conditions governed the design of the prototype bridge in positive and negative bending at Overload. The AASHTO lane loading plus impact governed in negative bending and, therefore, had to be used to cause local yielding at interior-pier sections in the model bridge to form the automoments. The AASHTO truck loading plus impact governed in positive bending and, therefore, had to be used to check the maximum stresses in positive bending in the model bridge after formation of the automoments. Because only the 18 concentrated load points, used to apply the compensatory dead loads, were available to load the model bridge as shown in Fig. 18, it was not possible to exactly simulate the AASHTO uniform lane load and each axle of an AASHTO HS truck in the model-bridge test. The fact that the model bridge was a three-dimensional structure complicated matters as well. Therefore, approximations had to be made. It was decided to simulate these live loadings by applying a set of concentrated loads at the available load points that would give approximately the same critical elastic live-load moments and shears as the actual AASHTO HS20 Overload lane and truck loadings plus impact would give in each girder of the model bridge. This in itself is an approximation because the model bridge is not elastic at Overload prior to shakedown. It was felt, however, that these elastic moments and shears would still be a reasonable benchmark for determining the applied loads.

The first step was to determine the critical elastic live-load moments and shears in each girder of the model bridge due to the actual AASHTO HS20 loadings plus impact, using the three-dimensional MSC/NASTRAN finite-element model of the model bridge. All loads were scaled down as required based on the 0.4 scale factor. The AASHTO load (beta) factor of 5/3 and AASHTO impact factor were included. Pressure loadings were used to apply the scaled-down uniform Overload lane loading over a 4-ft wide design lane (10-ft lane scaled down) in both spans of the finite-element model. A scaled-down concentrated load was included at the six-tenth points in each span (measured from the abutments) for the lane loading as specified by AASHTO. Truck loading was applied in one span only. For loading of an exterior girder, the finite element model was loaded with two lanes of scaled-down AASHTO Overload lane and truck loading plus impact. In the prototype design, two lanes loaded was determined to give the most critical live-load distribution to the exterior girders for this particular bridge configuration, Table 2. The loads were shifted over in the design lanes according to AASHTO rules to cause the worst loading on the exterior girder. Statically equivalent loads were used so the loads and pressures could be applied directly on the nodes and elements of the finite-element model. For the interior girder, three

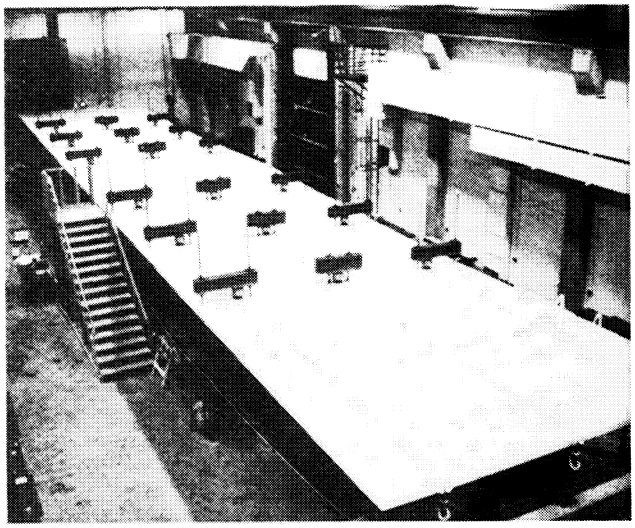

Fig. 18. Photograph of model bridge during application of simulated Overload with load fixtures on top of bridge.

lanes of loading were determined to give the most critical live-load distribution, Table 2, and therefore three lanes of scaled-down AASHTO Overload lane and truck loading plus impact were applied to the finite-element model.

The next step was to determine a set of concentrated loads that would give approximately the same critical elastic live-load moments and shears in the model bridge as the actual scaled-down AASHTO loadings. The elastic influence surfaces for critical moments and shears in the model bridge were available from the finite-element model. Using these surfaces and a trial-and-error approach, a reasonable set of concentrated loads was computed for each case. For simulation of the AASHTO lane loading, the line of concentrated loads directly over the loaded girder (exterior or interior) was made slightly larger. When loading for negative bending in continuous spans, AASHTO requires that a concentrated load in each span be included with the uniform lane load, located to produce the maximum effect. Therefore, the concentrated loads at the six-tenth points in each span on each girder were made slightly larger than the other loads on that girder to more closely resemble the configuration of the AASHTO lane loading. For simulation of the AASHTO truck loading, the concentrated loads were applied in one span only.

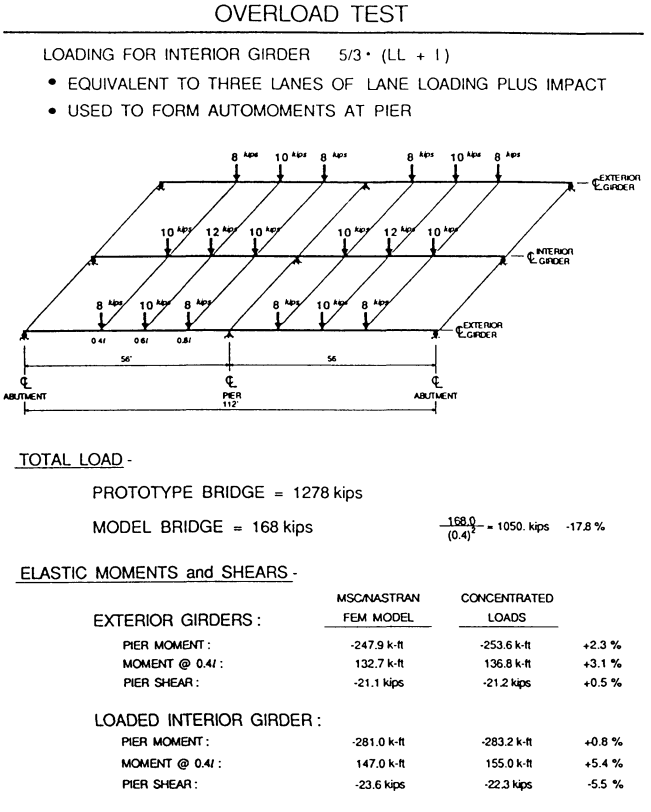

Fig. 19. Equivalent concentrated loads used to simulate three lanes of AASHTO HS20 Overload lane loading plus impact for critical loading of the interior girder.

The concentrated loads used to model three lanes of AASHTO HS20 Overload lane loading plus impact for critical loading of the interior girder (to form the automoments) are shown in Fig. 19. The concentrated loads applied to model three lanes of AASHTO HS20 Overload truck loading plus impact for critical loading of the interior girder and used to check the maximum stress in positive bending in the interior girder are shown in Fig. 20. Similar loads for critical loading of the exterior girders are not shown. Also given in each figure are comparisons of the computed critical elastic live-load moments and shears in selected girders of the model bridge, due to the indicated concentrated test loads and due to the associated scaled-down AASHTO Overload loadings on the finite-element model (labeled MSC/NASTRAN FEM MODEL). The agreement was considered to be satisfactory. All loads and moments indicated in Figs. 19 and 20 for the critical interior-girder loading should have been reduced by 10 percent. As mentioned, AASHTO allows this reduction when three lanes are loaded to account for the probability of coincident loading. However, it will be shown later that all these loads eventually had to be increased above their indicated levels. Thus, this accidental oversight had a negligible effect.

The critical interior-girder live loading was applied first. The simulated truck- and lane-load patterns were applied alternately in that order for several cycles. During each cycle, the live loads were applied on top of the total compensatory dead loads at each location in increments in the given ratios

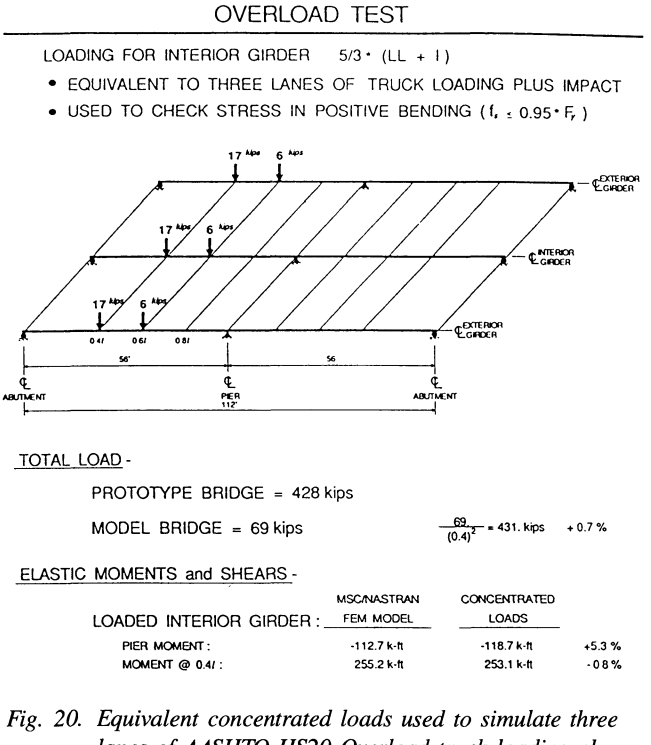

Fig. 20. Equivalent concentrated loads used to simulate three lanes of AASHTO HS20 Overload truck loading plus impact for critical loading of the interior girder.

using a load maintainer up to 100 percent of the specified live loads. Each set of live loads was then unloaded, but the compensatory dead loads were never unloaded. The specified live loads at 100 percent were initially computed by reducing the calculated loads, shown in each figure, to account for the fact that the measured static yield strength of the bottom-flange plate material at the critical positive-moment section in the interior girder was below the specified nominal yield strength of 50 ksi. All live loads were reduced by a constant ratio of the measured static yield strength of the bottom-flange plate at the critical positive-moment section in the girder to the nominal yield strength. The dead loads were not reduced by this ratio. Because of the reduction, the loading more closely represented rated AASHTO Overload vehicles. After five cycles of alternate truck and lane loading at this approximate rated load level, the measured maximum stress in positive bending in the interior girder was only approximately $0.85F_y$. The low stress level was partially due to the unintentional reduction in the compensatory dead load during installation of the precast panels. Subsequently, the simulated truck and lane loads were both increased in the given proportions by approximately 32 percent, and the load cycles were repeated at this load level. It was estimated that the measured maximum stress in positive bending in the most heavily loaded girder would be approximately $0.95F_y$ after several cycles of alternate loading at this higher level.

After the critical interior-girder loading at the higher level was completed, the critical exterior-girder loadings were then similarly applied over each exterior girder at the same higher level to shake down the entire bridge.

Test Results

The total measured vertical deflections for each load cycle at midspan of the west span of the interior girder at the higher level of critical interior-girder live loading are shown in Fig. 21. Total deflections under the simulated Overload lane and truck loadings are shown for each cycle. The deflections began to stabilize after about the third cycle of loading indicating that shakedown had occurred. The larger deflection under the simulated lane loading in cycle 3 was due to slightly heavier live loads being unintentionally applied during that cycle. The bridge was still able to shake down. The measured maximum stress in positive bending in the interior girder under the simulated truck loading increased with each load cycle early on indicating the presence of automoments. The measured maximum stress in the interior girder stabilized at approximately $0.95F_y$ after about three cycles of loading at the higher level. The behavior was similar under the critical exterior-girder loading.

The summations of the measured dead-load reactions at each bearing line before and after the start of the critical interior-girder loading are given in Fig. 22. The difference in the reactions before and after Overload testing at each bearing line can be considered to be the autoforces, or reactions, due to the automoments illustrated in Fig. 17. The autoforces could have been directly measured if it were possible to unload all the dead load. The average of the total automoment reactions at the end abutments was approximately equal to half the total interior-pier automoment reaction, as required by statics. The end-abutment automoment reactions were not symmetrical because fabrication tolerances of the cross frames resulted in unequal distribution of the steel dead weight when the bridge was erected, and the problem magnified somewhat as the loads increased. The average total automoment end-abutment reaction times the span length gave a total positive automoment across the interior-pier bearing line of 201.7 kip-ft. This total pier automoment represented about 8.7 percent of the sum of the total elastic Overload pier moments in each girder across the interior-pier bearing line in the prototype bridge (scaled down). This illustrates that the automoments are essentially a theoretical refinement of the ten-percent moment redistribution presently allowed in LFD at Overload for bridges utilizing compact sections. The sum of the calculated interior-pier automoments in each girder used in the design of the prototype bridge at Overload (scaled down) was conservatively equal to 454.4 kip-ft.

Figure 23 is a photograph of the interior-pier region of one exterior girder in the model bridge at the completion of all the Overload testing and after shakedown at the limit state in each girder at the higher load level. There were very

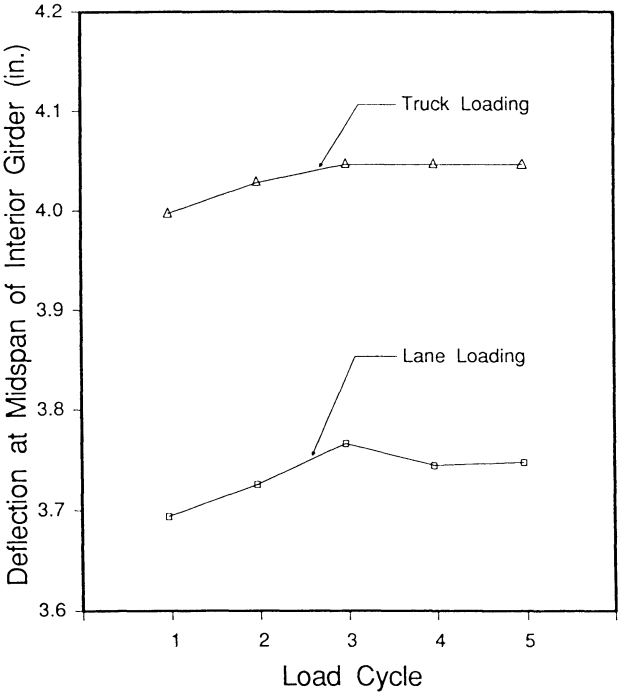

Fig. 21. Total measured vertical deflection at midspan of the interior girder in the west span during repeated application of the simulated Overload.

slight increases in the deformations of the girder webs and bottom (compression) flanges. Some distortion of the flange and web plates had occurred during fabrication of the girders. It was felt these small additional deformations would have been controlled by the closely spaced stiffeners that were added to the girders before the Maximum Load testing. Selected Overload tests, repeated after installation of these stiffeners, confirmed this opinion.

Cracking of the precast panels was observed only in the panel directly over the interior pier. The observed cracks were less than 7 mils (.007 in.) wide and closed when the live load was removed. The cracks were generally observed to initiate from the corners of the grouted blockouts. There were no cracks observed in the adjacent panel-to-panel joints. After all girders had shaken down with the maximum stress in positive bending in the most heavily loaded girder at approximately $0.95F_y$, the girder camber, which included the anticipated camber due to the automoments, was essentially zero. Thus, the ALFD limit-state criteria appeared to do a satisfactory job of satisfying the Overload structural performance requirement.

MAXIMUM LOAD TESTING

The single structural performance requirement at Maximum Load is that the bridge be able to safely resist the load. ALFD procedures introduce the concept of plastic-design mechanism analysis to continuous-bridge design to satisfy this requirement. According to the ALFD guide specification, it is assumed in the mechanism analysis that sections where the first hinges form, normally the interior-pier sections, rotate inelastically at a constant moment termed the effective plastic moment, M_{pe}.[16] M_{pe} is a reduced plastic moment computed from the section geometry. The reduced M_{pe} is used in the mechanism analysis because most sections used in bridge design do not qualify as compact according to conventional AISC plastic-design rules.[17] At M_{pe}, a section can be considered to have adequate inelastic rotation capacity to allow the Maximum Load moment to redistribute longitudinally to more lightly loaded positive-moment sections before those sections reach their ultimate capacities, creating a mechanism.

Research is presently in progress to determine how much inelastic rotation capacity is available in non-compact girders with slender webs in negative bending at different levels of M_{pe}.[7,9] Because the prototype non-compact girders had to be designed before this research was under way, it was decided to use the M_{pe} level defined by the guide specification for braced compact sections in the mechanism analysis at Maximum Load. Levels of M_{pe} to be used for non-compact girder sections will be established in this related AISI research.

To attempt to verify that the model-bridge girders would have sufficient inelastic rotation capacity at this level of M_{pe} and at the corresponding level of shear, a component specimen representing the interior-pier region of one of the model-bridge girders was built and tested.[10] The component specimen was a single simple-span 0.4 scale composite girder, with

MAXIMUM LOAD TEST

LOADING FOR EXTERIOR GIRDER 1.3• [5/3• (LL + I)]

- EQUIVALENT TO TWO LANES OF LANE LOADING PLUS IMPACT
- USED TO CHECK FOR MECHANISM

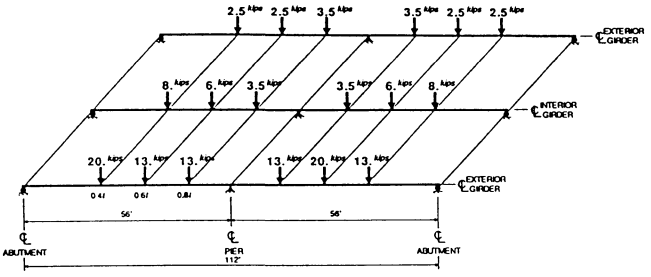

TOTAL LOAD -

PROTOTYPE BRIDGE = 1108 kips

MODEL BRIDGE = 144 kips $\quad \frac{144.0}{(0.4)^2} = 900$ kips -18.7 %

ELASTIC MOMENTS and SHEARS -

LOADED EXTERIOR GIRDER:	MSC/NASTRAN FEM MODEL	CONCENTRATED LOADS	
PIER MOMENT:	-368.0 k-ft	-385.1 k-ft	+4.7 %
MOMENT @ 0.4l:	231.2 k-ft	229.5 k-ft	- 0.7 %
PIER SHEAR:	-30 9 kips	-31.4 kips	+1.8 %
INTERIOR GIRDER:			
PIER MOMENT:	-240.9 k-ft	-233.1 k-ft	- 3.2 %
MOMENT @ 0.4l:	155.7 k-ft	144.5 k-ft	- 7.2 %
PIER SHEAR:	-19 6 kips	-16.7 kips	- 14 7 %

Fig. 22. Summation of dead-load reactions at each bearing line before and after the simulated Overload for critical loading of the interior girder.

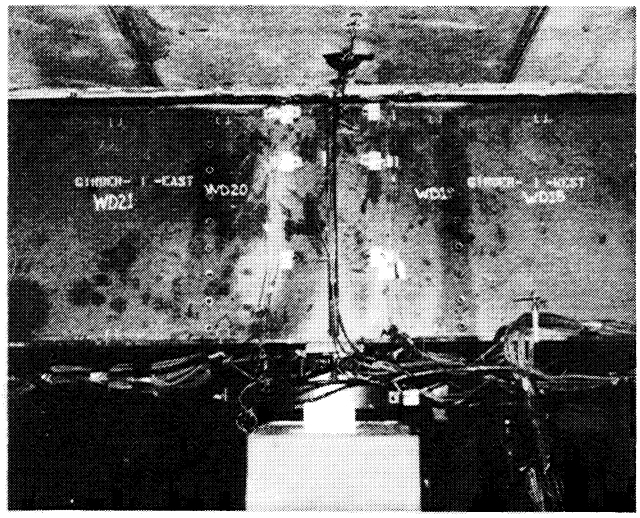

Fig. 23. Photograph of interior-pier region of an exterior girder after completion of Overload testing.

precast panels post-tensioned parallel to the supporting girder, approximately simulating the middle field section of the model-bridge girders. The specimen had an ultracompact bottom (compression) flange but did not have the closely spaced transverse stiffeners adjacent to the interior pier, mentioned earlier. Downward load was applied at the specimen ends and held in the steel beam prior to panel erection and grouting to simulate the noncomposite dead-load pier moment in the model bridge. After erection and grouting of the panels, testing in negative bending was continued to determine the full inelastic moment-rotation curve.

From the component test, it was determined that the inelastic rotation capacity of the pier section at its computed M_{pe} was slightly greater than the theoretical required rotation at Maximum Load in the model bridge. The component specimen was also able to achieve a maximum shear force at the interior pier in the test greater than the theoretical Maximum Load pier shear forces anticipated in the continuous model-bridge girders at Maximum Load. It was later decided, after the model bridge was constructed, to add the closely spaced transverse stiffeners to each of the model-bridge girders before the Maximum Load testing to further improve the rotation capacity. It was also felt this additional stiffener was needed since the component test could not account for the effect of yielding in positive bending, which causes additional inelastic rotation at the pier.

To determine the adequacy of the plastic mechanism analysis using M_{pe} for the strength prediction of a continuous bridge at Maximum Load, it was decided to subject the model bridge to a simulated rated AASHTO Maximum Load lane loading. For this particular bridge configuration, lane loading was determined to be more critical for mechanism formation because it causes larger rotations at the interior pier than truck loading. After adding load to compensate for the compensatory dead load that was lost during erection of the precast panels, and additional dead load (DL3) to simulate the theoretical 30 percent in dead load specified by AASHTO at Maximum Load, the simulated lane loads were increased in increments until the measured critical bottom-flange bending stress in the positive-moment region of the most heavily loaded girder equaled the static yield stress. This represented the LFD limit state for non-compact girders in positive bending at Maximum Load and represented the rated load. The loads were then increased further in the given proportions to determine how much reserve strength was available in the bridge above the rated load. Simulated lane loads for critical loading of each girder were also applied.

Development of Applied Loads

The same procedure described earlier to simulate the Overload lane loading plus impact was used to simulate the AASHTO HS Maximum Load lane loading plus impact. The same 18 concentrated load points were used. The line of concentrated loads directly over the loaded girder (exterior or interior) was again made slightly larger. However, in this case, the concentrated loads at the four-tenths point in one span and the six-tenths point in the other span were made slightly larger than the other loads on the most heavily loaded girder. This represented a slight deviation from the configuration of the simulated Overload lane loads but was felt to represent the most critical lane-loading configuration for mechanism formation. The concentrated loads used to simulate two lanes of AASHTO HS20 Maximum Load lane loading plus impact for critical loading of an exterior girder are shown in Fig. 24. Also given in Fig. 24 is a comparison of the computed critical elastic live-load moments and shears in selected girders of the model bridge due to the indicated concentrated test loads and due to the associated scaled-down AASHTO Maximum Load loadings on the finite-element model (labeled MSC/NASTRAN FEM MODEL). The agreement was again considered to be satisfactory. Similar load patterns for critical loading of the interior girder and the other exterior girder are not shown. In developing these loads, the 10 percent reduction factor allowed by AASHTO to account for the probability of coincident loading was considered in computing the loads for critical loading of the interior-girder, which simulated three lanes loaded.

After applying the additional dead loads, the critical

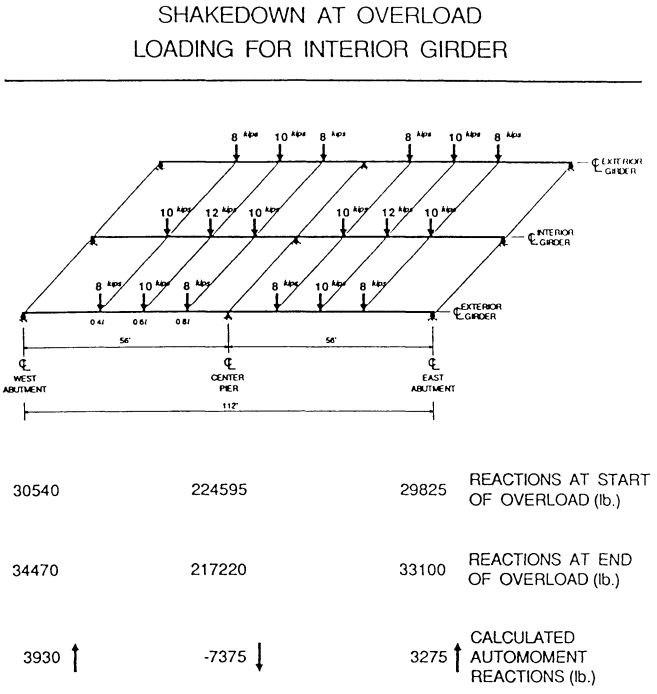

Fig. 24. Equivalent concentrated loads used to simulate two lanes of AASHTO HS20 Maximum Load lane loading plus impact for critical loading of an exterior girder.

interior-girder live loading was applied first. The live loads were again applied on top of the total compensatory dead loads at each location in increments in the given ratios using the load maintainer up to 100 percent of the specified live loads. The specified live loads, at 100 percent, were computed by reducing all calculated loads by the constant ratio of the actual measured static yield strength of the bottom-flange plate material in the positive-bending region to the specified nominal yield strength, as was done in the Overload tests to more closely represent rated vehicles.

After these approximate rated loads were applied for critical loading of the interior girder, a set of rated loads was computed and applied for critical loading of an exterior girder. The loads were then increased above the rated loads in the given ratios. An exterior girder was loaded above the "rated" loads first because it was felt this would be the more critical case. This same procedure was then followed for the other exterior girder. Finally, the critical loading for the interior girder was applied again, only this time the loads were increased above the rated loads. In between each test, only the live loads were unloaded.

Test Results

Under the first application of the approximate rated loads for critical loading of the interior girder, the maximum measured bottom-flange stress in the positive-moment region of the interior girder was approximately equal to the static yield stress. Deformations in the steel girders were barely visible at this load level and included some additional compression-flange and web deformation in each girder adjacent to the interior pier. This had no effect on the ability of the structure to safely carry the load.

Under the approximate rated loads for critical loading of the first exterior girder, the maximum measured bottom-flange stress in the positive-moment region of that girder was again approximately equal to the static yield stress. Figure 25 shows a plot of the total load (dead plus live load) versus the measured vertical deflections at midspan of the west span of the exterior girder and the interior girder for the critical exterior-girder loading as the loads were then increased above the rated loads. The simulated "rated" Maximum Load level is indicated in the figure. The plot illustrates the tremendous reserve capacity that was available above the rated loads. The bridge was able to sustain total additional live load approximately 240 percent above the rated live load before reaching the limit of jack capacity. Figure 26 shows the bridge at this level of live load 240 percent above the rated live load. The deformations in the steel girders adjacent to the interior pier gradually increased with the load, but the bridge was still able to sustain the increased load. As expected, additional cracking was observed in the precast panels over and adjacent to the interior pier. However, serviceability of the bridge is not a concern at Maximum Load. No crushing of the concrete panels was observed in positive-moment regions.

Loads were then applied for critical loading of the other exterior girder, and similar behavior was observed. The bridge sustained a total live load approximately 220 percent above the rated live load before the test was stopped. Finally, higher capacity jacks were installed at selected load points and the critical interior-girder loading was reapplied. The bridge then sustained a total live load approximately 250 percent above the rated live load before concrete crushing was observed in the deck panel at the four-tenths point in the west span ending the test.

This series of Maximum Load tests indicated that significant transverse load sharing occurs among steel girders in a cross section as they are loaded well into the inelastic range.

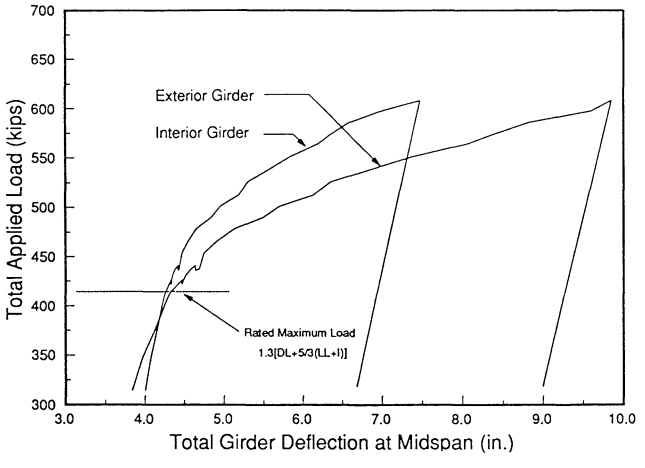

Fig. 25. Deflection at midspan of the west span of the interior and exterior girders during Maximum Load test for critical exterior-girder loading.

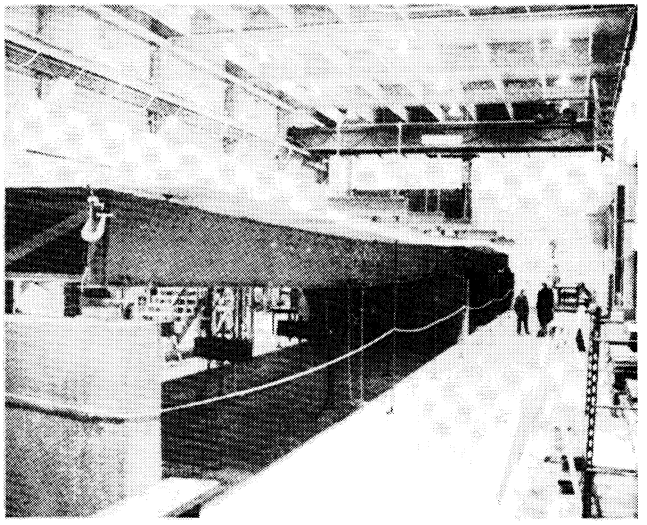

Fig. 26. Photograph of model bridge at 240 percent of the rated AASHTO HS20 Maximum Load.

This load sharing is not adequately accounted for by using an elastic lateral wheel-load distribution factor in Maximum-Load design procedures. This transverse load sharing, along with the available strength in the positive-moment regions, coupled with the adequate available rotation capacity in the negative-moment regions, helped account for the observed reserve strength. The ALFD limit-state criteria were more than adequate to meet the Maximum Load performance requirement for this bridge.

CONCLUSION

A large experimental test program to evaluate the behavior of a two-span continuous 0.4 scale model of a plate-girder bridge, with precast prestressed modular concrete deck panels, designed according to Alternate Load Factor Design (ALFD) or Autostress Design procedures has recently been completed. The bridge was designed using non-compact plate girders with slender webs that fall beyond the present limits of the ALFD guide specification. A comprehensive plan was followed to subject the model bridge to a series of tests to evaluate specific responses at simulated Service Load, Overload, and Maximum Load levels.

At elastic Service-Load stress levels, live-load lateral-distribution factors for the exterior and interior girders in positive and negative bending were computed from experimentally developed influence surfaces. These factors were compared to factors computed from a finite-element model, from proposed empirical formulas, and from present AASHTO procedures. The agreement between the factors computed from the experimental and MSC/NASTRAN data was generally good. The factors computed from the proposed empirical formulas also gave good agreement with experimental data, especially for the interior girder. However, the proposed formulas did not differentiate between two- and three-lanes loaded. The factors computed using present AASHTO procedures were quite conservative for the interior girder and less so for the exterior girders. Neither the proposed nor the present AASHTO procedures accounted for the observed variation of the distribution factor along the span. The data would seem to indicate that finite-element analysis is a very plausible method for computing elastic wheel-load girder distribution factors.

At Overload, shakedown with the formation of automoments was experimentally observed. Shakedown (elastic behavior) occurred after about three cycles of alternating simulated Overload truck and lane loading, with the maximum stress in positive bending in the most heavily loaded girder at approximately the limit state of $0.95F_y$. The girders behaved satisfactorily, even with controlled local yielding allowed at interior piers. The precast prestressed modular panels behaved exceptionally well. Thus, the ALFD limit-state criteria appeared to adequately satisfy the Overload structural performance requirement of unobjectionable riding quality for this bridge, designed using non-compact girder sections. Refinements to the inelastic moment-rotation curve used to compute the automoments for non-compact girder sections will be made in upcoming related AISI research projects.

At Maximum Load, the bridge had significant reserve strength under simulated Maximum Load lane loading. The bridge was able to sustain three applications of a live load over two times the approximate rated Maximum Load live load. The ALFD plastic mechanism analysis using M_{pe} was adequate to ensure that this bridge had sufficient strength to resist the load. Levels of M_{pe} to use in the mechanism analysis for non-compact girder sections will also be established in ongoing related AISI research.

This paper was based on limited analysis of the numerous data available from this model-bridge test program. The data from this test program will continue to be analyzed and additional reports will be issued.

ACKNOWLEDGMENTS

The work reported in this paper was part of a cooperative investigation sponsored by the Federal Highway Administration (FHWA) and the American Iron and Steel Institute (AISI). The study was conducted under FHWA Contract No. DTFH61-83-C-00079 under the direction of Mr. Lloyd R. Cayes, Contracting Officer's Technical Representative, Federal Highway Administration, McLean, VA. Mr. Cayes has been assisted by Mr. Craig Ballinger and Ms. Sue Lane, Research Engineers, Mary McGrath, Contracting Officer, and the staff of the FHWA Structures Laboratory. Additional assistance in testing of the model bridge, reduction of test data, and data analysis efforts have been provided by Dr. Pedro Albrecht and Dr. Kamal Elnahal, of the University of Maryland, and Chi Associates, Inc., McLean, VA.

Design of the model bridge, load fixtures, instrumentation, and test plan was carried out by personnel from the steel industry and by Wiss, Janney, Elstner Associates, Inc. (WJE), retained by AISI to coordinate the technical aspects of the project. A. C. Kuentz of AISI and M. E. Moore of WJE served as co-principal investigators during the model bridge study. The staff of the study included M. A. Grubb of AISC Marketing, Inc., R. P. Knight with Dynamic Isolation Systems formerly of Bethlehem Steel Corp., R. W. Lautensleger of ARMCO, and K. A. Strand of WJE.

The entire project was under the guidance of an AISI Advisory Panel. The members of this panel were J. M. Barsom of USS, a division of the USX Corporation, Chairman, R. S. Fountain of Parsons-Brinckerhoff, G. Haaijer of the American Institute of Steel Construction, E. V. Hourigan of Parsons-Brinckerhoff formerly of the New York DOT, C. L. Loveall of the Tennessee DOT, R. L. Mion of AISC Marketing, Inc., B. T. Yen of Lehigh University, P. Zia of North Carolina State University, and I. M. Viest of Bethlehem, PA.

Fabrication and erection of the model bridge was completed by Atlas Machine and Iron Works, Gainesville, VA.

Precast components were fabricated by Shockey Bros. of Winchester, VA and post-tensioning completed by VSL Corp., Springfield, VA. Load fixtures for the model bridge were fabricated by Salisbury Steel, Salisbury, MD.

REFERENCES

1. Haaijer, G., Carskaddan, P. S., Grubb, M. A., "Suggested Autostress Procedures for Load Factor Design of Steel Beam Bridges," Bulletin No. 29, American Iron and Steel Institute, Washington, DC, April 1987.
2. Grubb, M. A., "The AASHTO Guide Specification for Alternate Load Factor Design Procedures for Steel Beam Bridges Using Braced Compact Sections," *Engineering Journal,* American Institute of Steel Construction, Chicago, IL, Vol. 24, No. 1, First Quarter 1987.
3. *Guide Specification for Alternate Load Factor Design Procedures for Steel Beam Bridges Using Braced Compact Sections,"* American Association of State Highway and Transportation Officials, Washington, DC, 1986.
4. Loveall, C. L., "Advances in Bridge Design and Construction," Proceedings of the National Engineering Conference, Nashville, TN, American Institute of Steel Construction, Chicago, IL, June 12–14, 1986.
5. Holt, R. C., Hourigan, E. V., "Design of a Rolled-Beam Bridge by New AASHTO Guide Specification for Braced Compact Sections," Proceedings of the National Engineering Conference, Nashville, TN, American Institute of Steel Construction, Chicago, IL, June 12–14, 1986.
6. Vasseghi, A., Frank, K. H., "Static Shear and Bending Strength of Composite Plate Girders," Final Report AISI Project 320A, Phil M. Ferguson Structural Engineering Laboratory Report No. 87-4, University of Texas, Austin, TX, June 1987.
7. Schilling, C. G., "Moment-Rotation Tests of Steel Bridge Girders," AISI Project 188, American Iron and Steel Institute, Washington, DC, April 15, 1985.
8. Schilling, C. G., "Exploratory Autostress Girder Designs," AISI Project 188, American Iron and Steel Institute, Washington, DC, July 1986.
9. Schilling, C. G., Marcos, S. S., "Moment Rotation Tests of Steel Girders with Ultracompact Flanges," AISI Project 188, American Iron and Steel Institute, Washington, DC, July 1988.
10. Knight, R. P., Grubb, M. A., Moore, M. E., "Model Bridge with Precast Deck Panels," Proceedings of the National Engineering Conference, Nashville, TN, American Institute of Steel Construction, Chicago, IL, June 12–14, 1986.
11. Moore, M. E., Viest, I. M., "Laboratory Tests of a Continuous Composite Bridge," Proceedings of Conference on Composite Construction of Steel and Concrete, Henniker, N. H., American Society of Civil Engineers, New York, NY, June 1987.
12. *Standard Specifications for Highway Bridges,* The American Association of State Highway and Transportation Officials, Washington, DC, Thirteenth Edition, 1986.
13. Imbsen & Associates, Inc., "Distribution of Wheel Loads on Highway Bridges," unpublished report of NCHRP Project 12-26, Transportation Research Board, Washington, DC.
14. Knight, R. P., "Economical Steel Plate Girder Bridges," *Engineering Journal,* American Institute of Steel Construction, Chicago, IL, Second Quarter 1984.
15. McCormick, C. W., Editor, "MSC/NASTRAN User's Manual," The MacNeal-Schwendler Corporation, Los Angeles, CA.
16. Carskaddan, P. S., Haaijer, G., Grubb, M. A., "Computing the Effective Plastic Moment," *Engineering Journal,* American Institute of Steel Construction, Chicago, IL, First Quarter 1982.
17. "Specification for the Design, Fabrication, and Erection of Structural Steel for Buildings," Eighth Edition, American Institute of Steel Construction, Chicago, IL, November 1, 1978.
18. Branson, D. E., *Deformation of Concrete Structures,* McGraw-Hill International, 1977.
19. Montgomery, S. L., Frank, K. H., "Fatigue and Ultimate Strength of a Transversely Stiffened Plate Girder," Final Report AISI Project 320A Phase II, Phil M. Ferguson Structural Engineering Laboratory Report No. 87-7, University of Texas, Austin, TX, November 1987.
20. Carskaddan, P. S., Grubb, M. A., "Live-Load Lateral Distribution for the Approach Spans for the Cooper and Wando Rivers Bridge," U.S. Steel Research Bulletin, June 16, 1983.